

Distributed Predictive Control for Frequency and Voltage Regulation in Microgrids

Juan S. Gómez¹, Doris Sáez², *Senior Member, IEEE*, John W. Simpson-Porco³, *Member, IEEE*,
and Roberto Cárdenas⁴, *Senior Member, IEEE*

Abstract—Distributed control schemes have transformed frequency and voltage regulation into a local task in distributed generators (DGs) rather than by a central secondary controller. A distributed scheme is based on information shared among neighboring units; thus, the microgrid performance is affected by issues induced by the communication network. This paper presents a distributed predictive control applied to the secondary level of microgrids. The model used for prediction purposes is based on droop and power transfer equations; however, communication features, such as connectivity and latency, are also included, thus making the controller tolerant to electrical and communication failures. The proposed controller considers the frequency and voltage regulation control objectives and consensus over the real and reactive power contributions from each power unit in the microgrid. The experimental and simulation results show that the proposed scheme (i) responds properly to load variations, working within operating constraints, such as generation capacity and voltage range; (ii) maintains the control objectives when a power unit is disconnected and reconnected without any user updating in the controllers; and (iii) compensates for the effects of communication issues over the microgrid dynamics.

Index Terms—Secondary control, distributed predictive control, microgrids, constrained optimization, plug-and-play controller.

I. INTRODUCTION

MICROGRIDS are more sensitive than large-scale power systems to small changes in either load balance or power capacity. Currently, the microgrid community accepts that a distributed secondary control level is inherently fault tolerant to such electrical issues [1]. However, each controller

in a distributed scheme should be able to calculate its control action according to its knowledge about the current state of the microgrid. The necessity of updating the microgrid knowledge implies good communication among the controllers; therefore, the communication performance and the microgrid performance are directly related.

In [2] and [3], information shared through the communication network updates an electrical model used by each secondary controller. This model is based on the microgrid admittance matrix and is applied to an optimization problem to achieve a stable operation point for frequency and voltage when any DG is either plugged in or unplugged. In this case, the electrical model is adjusted, without any user intervention, according to Kirchhoff's voltage law when some change occurs in the microgrid. This feature is called plug-and-play (PnP) capability.

A second approach to include the microgrid model at the secondary control level is a graph-based representation of the information flow among the DGs. In this case, the DGs are represented as graph vertices, and the communication links are represented as graph edges. A weighted matrix that represents the graph connectivity among DGs is called the adjacency matrix. This matrix permits the exploration of the properties of the network systems [4]. In [5], a distributed consensus problem is applied over the microgrid. It is shown that the problem converges if and only if the microgrid graph has a path between any two DGs (connected graph), and the final value is the average of the initial conditions of the consensus variables.

One application of consensus in microgrids is the distributed averaging proportional-integral (DAPI) controller proposed in [6]. This scheme adds a term to the proportional-integral (PI) secondary controllers to achieve real power consensus for the frequency loop and reactive power consensus for the voltage loop. The DAPI controller is considered to be a PnP controller because the adjacency matrix can be updated online, and then, the control law changes if a DG is connected to or disconnected from the microgrid. However, this controller is not robust against communication issues, such as data dropouts or latency issues, because its control law only considers current information.

Communication issues are not uncommon in networks because communication links are susceptible to external factors such as weather, obstructions and interference. Data latency, data losses, and network topology changes generally degrade the control performance irrespective of the technology or topology used in the network [7].

Manuscript received March 7, 2019; revised July 8, 2019; accepted August 11, 2019. Date of publication August 16, 2019; date of current version February 19, 2020. This work was supported in part by the Fondo Nacional de Desarrollo Científico y Tecnológico (FONDECYT) under Grant 1170683, in part by the Complex Engineering Systems Institute (CONICYT - PIA - FB0816), in part by the Solar Energy Research Center SERC-Chile (CONICYT/FONDAP/ Project under Grant 15110019), and in part by the National Science and Engineering Research Council of Canada (NSERC) Discovery under Grant RGPIN-2017-04008. The work of J. S. Gómez was supported by the Ph.D. Scholarship from the Comisión Nacional de Investigación Científica y Tecnológica CONICYT-PCHA/Doctorado Nacional para extranjeros/2015-21150555. Paper no. TSG-00339-2019. (*Corresponding author: Doris Sáez.*)

J. S. Gómez, D. Sáez, and R. Cárdenas are with the Department of Electrical Engineering, University of Chile, Santiago 8370451, Chile (e-mail: jugomez@ug.uchile.cl; dsaez@ing.uchile.cl; rcardenas@ing.uchile.cl).

J. W. Simpson-Porco is with the Department of Electrical and Computer Engineering, University of Waterloo, Waterloo, ON N2L 3G1, Canada (e-mail: jwsimpson@uwaterloo.ca).

Color versions of one or more of the figures in this article are available online at <http://ieeexplore.ieee.org>.

Digital Object Identifier 10.1109/TSG.2019.2935977

In [6], an updated adjacency matrix used by the DAPI controller permits changes in the communication network topology to be addressed, therein preserving the frequency and voltage regulation. In [8], latency effects in the frequency restoration loop are compensated by a PI controller with a Smith predictor. To tune this, a constant delay estimation is used; however, the real delay in communication networks is not fixed. To solve this issue, in [9], a centralized PI controller with gain scheduling for frequency restoration is used to change the tuned point when the delay also changes.

A set of consensus-based controllers that ensure convergence for regulation and power sharing in a finite time have recently been reported. These PnP controllers have shown good performance against latency and communication path failures. In [10], two decoupled finite-time controllers that preserve the frequency-real power and voltage-reactive power relations are compared with a centralized controller using a six-DG microgrid. Conversely, in [11], four independent finite-time controllers are used by each DG to regulate frequency and voltage and to achieve real and reactive power sharing. The stability analysis of this scheme ensures convergence irrespective of the latency in the network.

The use of predictive control at the secondary level in microgrids is a promising approach because it is possible to address data dropouts and latency issues [12]. In [8], a centralized predictive controller is implemented to regulate the frequency in a microgrid with two DGs, therein achieving better latency compensation than with the Smith predictor. Furthermore, if predictive control is combined with a distributed scheme, it is possible to include PnP capability [13]. The challenge to implementing predictive controllers at the secondary level of microgrids is defining an optimization problem that can be solved in a short sampling period.

In a distributed model-based predictive control (DMPC) scheme, a (discrete-time) system model is used by each controller to predict its self-behavior over a prediction horizon. The model used is based on local information (i.e., measurements) and shared information from other controllers (i.e., previously computed predictions), and it is introduced as a set of equality constraints into an optimization problem. The system solution minimizes a cost function based on the predicted trajectory and the information exchanged with other DGs. Although the optimal solution provides a sequence of control actions, only the first element is applied, and the optimization problem is solved again at the next sampling period (rolling horizon scheme) [14].

There are two methods used to solve the DMPC. Iterative methods optimize and share the result with other DMPCs several times within the time step. Noniterative methods perform optimization only once per time step to reduce the traffic over the communication network [15].

Three iterative DMPC schemes for frequency regulation in large-scale power systems are proposed in [16]. The model used for these controllers is based on the frequency-active power relationship, and these are compared with an automatic generation controller (AGC) and a centralized MPC (CMPC) over a communication network with the same topology as the electrical system. Because these schemes are iterative

schemes, they require considerable computational effort and a high-performance communication network; therefore, the implementation of these predictive controllers is expensive for actual microgrids.

In [17], [18], an unconstrained DMPC, which includes consensus, has been proposed for voltage regulation in microgrids. In [17], the state space model is used based on the PI, and droop controllers that are often used at the primary level. In this case, an analytical solution is achieved for voltage regulation, reducing the computational effort. In [18], this scheme is extended to cover communications issues whereas frequency regulation is achieved using a DAPI controller.

In [19], a DMPC for frequency regulation is proposed considering voltage range constraints and power sharing among neighbor microgrids. The prediction model is built assuming that the microgrid is composed of synchronous generators and wind turbines. In this case, one controller regulates the microgrid frequency and establishes a power consensus with neighbor microgrids, assuming ideal communications and fixed topology.

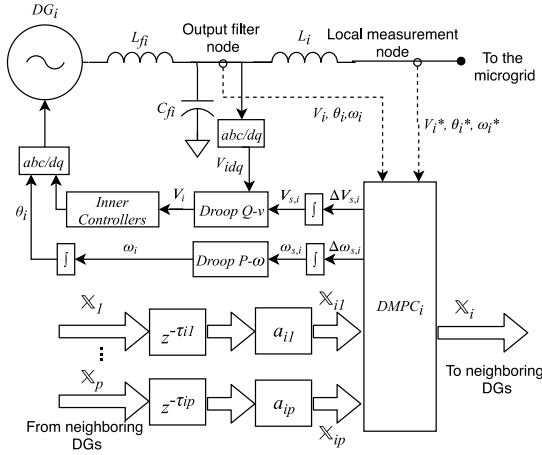
In [20], an iterative DMPC is proposed for frequency regulation and optimal economic dispatch. The optimization problem includes both the operation and maintenance costs for different types of DGs. In this case, consensus is not included because the power contributions are settled according to the cost and an ideal communication network is assumed, allowing information exchange several times per sampling period.

A. Paper Contributions

As shown, the PnP schemes using consensus techniques in addition to the regulation task (frequency and/or voltage) enable improved microgrid secondary level performance in several scenarios. However, we consider that predictive control has not been completely exploited for these applications. In this paper, we propose a noniterative DMPC that is capable of real-time operation in environments with communications issues, therein preserving the PnP capability.

The main advantage of the proposed DMPC controller is the model used to predict the microgrid behavior. Unlike previously reported DMPC for the secondary level of microgrids, the proposed model allows frequency and voltage regulation to be merged in the design of one multi-input multi-output distributed controller, and power consensus is achieved as well. This model is based on local voltage, frequency and power equations, including a communication network model that also represents connectivity and latency. The DMPC based on this model is updated on each DG once per sampling period with local measurements and with information shared from neighboring DGs. The proposed DMPC also includes explicit operational constraints such as voltage range and apparent power limits. Simulation and experimental results over heterogeneous microgrids validate the good performance of the proposed controller.

This paper is organized as follows. In Section II, the framework of the model used to build the optimization problem is presented. In Section III, the optimization problem used in the DMPC is detailed. The features of and parameters used in the

Fig. 1. DMPC_{*i*} diagram.

experimental setup, as well as the obtained results, are shown in Section IV. Section V presents remarks about the scalability of our proposal and a comparison with the DAPI scheme. The paper's conclusions and final remarks are presented in Section VI.

II. MODEL USED FOR CONTROL DESIGN

Considering that variables such as frequency, voltage, and real and reactive power are coupled in microgrids, the proposed model reflects this behavior based on droop, power transfer and phase angle equations. Additionally, a communication network model that considers the latency, defined by delay terms ($z^{-\tau_{ij}}$), and the connectivity, defined by adjacency terms (a_{ij}), is also proposed.

Because the model computes the power contribution of DG_{*i*} to the microgrid, external measurements are required. The voltage, frequency and phase angle are measured/estimated at the LC filter output (V_i , ω_i , θ_i) and at an adjacent measurement node (V_i^* , ω_i^* , θ_i^*). This adjacent measurement node is defined as the downstream node to the coupling inductance L_i .

The control scheme for DG_{*i*} in the microgrid is shown in Fig. 1. Note that the inner and droop controllers (primary level) work on a dq framework, whereas the $\omega_{s,i}$ and $V_{s,i}$ signals are droop inputs that compensate for voltage and frequency deviations. These signals and \mathbb{X}_i are from the proposed DMPC (secondary level), and these signals are computed as a solution to an optimization problem. \mathbb{X}_i is composed of frequency, voltage and power predictions, and it is shared with neighboring DGs using the communication network.

A description of each equation used to build the proposed model is included below, and the optimization problem and \mathbb{X}_i will be defined in Section III.

A. Droop Equations

Droop control provides statism to the microgrid, changing the operating point from the nominal frequency/voltage to ensure the real/reactive power supply when the microgrid is disturbed [21]. The droop control laws (1) and (2) define the linear frequency-real power and voltage-reactive power relations, respectively, where ω_0 and V_0 represent the nominal

frequency and voltage, $M_{p\omega,i}$ and $M_{qv,i}$ are the droop slopes, and $\omega_{s,i}$ and $V_{s,i}$ are the secondary control actions for unit i . Droop equations are included in the secondary control model because they determine the joint point between the primary and secondary control levels.

$$\omega_i(t) = \omega_0 + M_{p\omega,i}P_i(t) + \omega_{s,i}(t) \quad (1)$$

$$V_i(t) = V_0 + M_{qv,i}Q_i(t) + V_{s,i}(t). \quad (2)$$

B. Phase Angle Equation

Based on [22], the phase angle deviation ($\delta\theta_i$) generated for unit i by the coupling inductance L_i is defined by (3). The coupling inductance is a common passive element used to connect the low-pass filter output to the microgrid. For our controller, the phase angle deviation is required for estimating the real/reactive power transferred from the DG to the microgrid. To estimate $\delta\theta_i(t)$ properly, phase-locked loops (PLLs) should be placed at the output filter and the adjacent measurement node.

$$\delta\theta_i(t) = \theta_i(t) - \theta_i^*(t) = \int_0^t [\omega_i(\tau) - \omega_i^*(\tau)] d\tau. \quad (3)$$

C. Power Transfer Equations

To achieve power consensus in the microgrid, it is necessary to estimate the power contribution of each DG in the microgrid. In this case, our controller neglects the use of an admittance matrix-based model, as is generally used, to propose a model based on the power transferred through the coupling inductance. The equations that determine the power transferred from unit i to the microgrid are defined in (4) and (5), where $B_i = 1/L_i\omega_0$ [22].

$$P_i(t) = B_i V_i(t) V_i^*(t) \sin(\delta\theta_i(t)) \quad (4)$$

$$Q_i(t) = B_i [V_i(t)^2 - V_i(t) V_i^*(t) \cos(\delta\theta_i(t))]. \quad (5)$$

D. Discrete Time Model

Before deriving a predictive model, equations (1) to (5) are discretized using the forward Euler method, where $t_n = nT_{sec}$, $n \in \mathbb{Z}^+$, and T_{sec} is the sampling period used at the secondary control level. To eliminate the steady-state error, integrators are added at the DMPC outputs [14]; therefore, the incremental operator Δ , defined by (6), is applied to (1) and (2) to compute $\Delta\omega_{s,i}$ and $\Delta V_{s,i}$.

$$\Delta f(t_n) = [f(t_n) - f(t_{n-1})] \quad (6)$$

Additionally, a Taylor expansion is applied to (4) and (5) around the measured/estimated point $\{\omega_i(t_n), \omega_i^*(t_n), V_i(t_n), V_i^*(t_n), \delta\theta_i(t_n), P_i(t_n), Q_i(t_n)\}$, simplifying the optimization problem. The linear and discrete time model is shown in (7a).

$$\omega_i(t_{n+1}) = \omega_i(t_n) + M_{p\omega,i}[P_i(t_{n+1}) - P_i(t_n)] + \Delta\omega_{s,i}(t_n) \quad (7a)$$

$$V_i(t_{n+1}) = V_i(t_n) + M_{qv,i}[Q_i(t_{n+1}) - Q_i(t_n)] + \Delta V_{s,i}(t_n) \quad (7b)$$

$$\delta\theta_i(t_{n+1}) = \delta\theta_i(t_n) + T_{sec}[\omega_i(t_{n+1}) - \omega_i^*(t_n)] \quad (7c)$$

$$P_i(t_{n+1}) = P_i(t_n) + [V_i(t_{n+1}) - V_i(t_n)]B_i V_i^*(t_n) \sin(\delta\theta_i(t_n)) + [\delta\theta_i(t_{n+1}) - \delta\theta_i(t_n)]B_i V_i(t_n) V_i^*(t_n) \cos(\delta\theta_i(t_n)) \quad (7d)$$

$$\begin{aligned}
Q_i(t_{n+1}) &= Q_i(t_n) \\
&+ [V_i(t_{n+1}) - V_i(t_n)]B_i[2V_i(t_n) - V_i^*(t_n) \cos(\delta\theta_i(t_n))] \\
&+ [\delta\theta_i(t_{n+1}) - \delta\theta_i(t_n)]B_iV_i(t_n)V_i^*(t_n) \sin(\delta\theta_i(t_n)). \quad (7e)
\end{aligned}$$

E. Communication Network Model

In this work, a full-duplex communication network is considered in which the bidirectional link between units i and j is represented by an adjacency term a_{ij} and a delay term τ_{ij} . The adjacency term represents the connectivity between two units [6], defined by (8) in this work as a function of the received information on DG_i at each sampling period.

$$a_{ij}(t_n) = \begin{cases} 1 & \text{Data from } DG_j \text{ arrives to } DG_i \text{ at } t_n \\ 0 & \text{Data from } DG_j \text{ does not arrive to } DG_i \text{ at } t_n \\ 0 & j = i \end{cases} \quad (8)$$

The delay term ($\tau_{ij} \geq 1$) is measured in sampling periods, and this term represents the time required for the transmission-reception process between DG_i and DG_j . Because the communication is full duplex, the associated graph is undirected; thus, the equalities $\tau_{ij} = \tau_{ji}$ and $a_{ij} = a_{ji}$ are satisfied [4].

III. OPTIMIZATION FOR PREDICTIVE CONTROL

Predictive control optimizes a cost function using a set of equalities and inequalities as constraints that reflect the system behavior. The cost function and the constraints should be functions of the predicted variables. The optimal solution is a vector \mathbb{X} that contains the predicted values over the prediction horizon N_y and the control sequence over the control horizon N_u . For our controller, it is possible to use the set of equations (7a) to predict the DG behavior. Because controlled variables are explicit in the predictive model, it is possible to directly include operational constraints. The optimization problem and how it is solved are detailed below.

A. Predictive Model

The set of equations (7a) can be used to determine the DG behavior at t_{n+k} , where $k \in \mathbb{Z}^+$. Considering the linearization of (7d) and (7e) around the measured point at t_n , their coefficients are updated each sampling period and assumed to be constants through the prediction horizon in the optimization problem.

$$\begin{aligned}
\omega_i(t_{n+k}) &= \omega_i(t_{n+k-1}) + M_{p\omega,i}[P_i(t_{n+k}) - P_i(t_{n+k-1})] \\
&+ \Delta\omega_{s,i}(t_{n+k-1}) \quad (9a)
\end{aligned}$$

$$\begin{aligned}
V_i(t_{n+k}) &= V_i(t_{n+k-1}) + M_{qv,i}[Q_i(t_{n+k}) - Q_i(t_{n+k-1})] \\
&+ \Delta V_{s,i}(t_{n+k-1}) \quad (9b)
\end{aligned}$$

$$\delta\theta_i(t_{n+k}) = \delta\theta_i(t_{n+k-1}) + T_{sec}[\omega_i(t_{n+k}) - \omega_i^*(t_n)] \quad (9c)$$

$$\begin{aligned}
P_i(t_{n+k}) &= P_i(t_n) + [V_i(t_{n+k}) - V_i(t_n)]B_iV_i^*(t_n) \sin(\delta\theta_i(t_n)) \\
&+ [\delta\theta_i(t_{n+k}) - \delta\theta_i(t_n)]B_iV_i(t_n)V_i^*(t_n) \cos(\delta\theta_i(t_n)) \quad (9d)
\end{aligned}$$

$$\begin{aligned}
Q_i(t_{n+k}) &= Q_i(t_n) \\
&+ [V_i(t_{n+k}) - V_i(t_n)]B_i[2V_i(t_n) - V_i^*(t_n) \cos(\delta\theta_i(t_n))] \\
&+ [\delta\theta_i(t_{n+k}) - \delta\theta_i(t_n)]B_iV_i(t_n)V_i^*(t_n) \sin(\delta\theta_i(t_n)). \quad (9e)
\end{aligned}$$

B. Operational Constraints

The set of operational constraints is composed of equalities and inequalities included to ensure DG performance within the physical limits. This set of constraints is defined in (10a).

$$\bar{\omega}_i(t_{n+k}) = \frac{\omega_i(t_{n+k}) + \sum_{j=1}^p a_{ij}(t_n)\omega_j(t_{n+k-\hat{\tau}_{ij}})}{1 + \sum_{j=1}^p a_{ij}(t_n)} \quad (10a)$$

$$\bar{V}_i(t_{n+k}) = \frac{V_i(t_{n+k}) + \sum_{j=1}^p a_{ij}(t_n)V_j(t_{n+k-\hat{\tau}_{ij}})}{1 + \sum_{j=1}^p a_{ij}(t_n)} \quad (10b)$$

$$\bar{\omega}_i(t_{n+N_y}) = \omega_0 \quad (10c)$$

$$\bar{V}_i(t_{n+N_y}) = V_0 \quad (10d)$$

$$\bar{V}_{\min} \leq \bar{V}_i(t_{n+k}) \leq \bar{V}_{\max} \quad (10e)$$

$$\begin{aligned}
|P_i(t_n)| + |Q_i(t_n)| + \text{sign}(P_i(t_n))[P_i(t_{n+k}) - P_i(t_n)] \\
+ \text{sign}(Q_i(t_n))[Q_i(t_{n+k}) - Q_i(t_n)] \leq S_{\max} \quad (10f)
\end{aligned}$$

Note that equations (10a) and (10b), which define the frequency and voltage averages, include the parameters a_{ij} and $\hat{\tau}_{ij}$. Therefore, a_{ij} forces only the received information to be including in estimating and predicting the averages, providing robustness against communication path failures and data losses. $\hat{\tau}_{ij}$ represents the delay estimation in the communication process for compensating the network latency over the predicted averages.

Equations (10c) and (10d) force the average values to converge at the end of the prediction horizon N_y . Additionally, inequalities (10e) and (10f) ensure that the average voltage in the microgrid and the apparent power of DG_i remain within a specific range. Inequality (10f) is defined as a polytopic inner approximation of (11) using the triangular inequality.

$$|S_i(t)| = \left(P_i(t)^2 + Q_i(t)^2 \right)^{1/2} < S_{\max}. \quad (11)$$

C. Cost Function

The cost function (12) is built from six weighted terms, where each term represents a control objective in the microgrid. The first two terms represent the average frequency and average voltage regulation. Although the optimization problem is local for each DG, the regulation is global over the entire microgrid because these terms are based on predictions shared through the communication network. The third and fourth terms minimize the control action required by DG_i to achieve the control objectives. The last two terms find a consensus over the contribution of real and reactive power for neighboring DGs.

$$\begin{aligned}
J_i(t_n) &= \sum_{k=1}^{N_y} \left[\lambda_{1i}(\bar{\omega}_i(t_{n+k}) - \omega_0)^2 + \lambda_{2i}(\bar{V}_i(t_{n+k}) - V_0)^2 \right] \\
&+ \sum_{k=1}^{N_u} \left[\lambda_{3i}(\Delta\omega_{s,i}(t_{n+k-1}))^2 + \lambda_{4i}(\Delta V_{s,i}(t_{n+k-1}))^2 \right] \\
&+ \sum_{j=1, j \neq i}^p \sum_{k=1}^{N_y} \lambda_{5i} a_{ij}(t_n) \left(\frac{P_i(t_{n+k})}{|S_{i\max}|} - \frac{P_j(t_{n+k-\hat{\tau}_{ij}})}{|S_{j\max}|} \right)^2 \\
&+ \sum_{j=1, j \neq i}^p \sum_{k=1}^{N_y} \lambda_{6i} a_{ij}(t_n) \left(\frac{Q_i(t_{n+k})}{|S_{i\max}|} - \frac{Q_j(t_{n+k-\hat{\tau}_{ij}})}{|S_{j\max}|} \right)^2. \quad (12)
\end{aligned}$$

Algorithm 1 DMPC Solution for Each DG_i

Inputs: Measurements and estimations: $\{\omega_i(t_n), \omega_i^*(t_n), V_i(t_n), V_i^*(t_n), \delta\theta_i(t_n), P_i(t_n), Q_i(t_n)\}$
 Received information: $\mathbb{X}_{ij}, \forall j = \{1, \dots, p\}$

Outputs: $\mathbb{X}_i, \Delta\omega_{s,i}(t_n), \Delta V_{s,i}(t_n)$

Initialization:

- 1: Compute matrix coefficients of $H_i, F_i, A_i, A_{eq,i}, B_i, B_{eq,i}$
- 2: **for every** t_n **do**
- 3: Compute adjacency terms a_{ij} according to the received information.
- 4: According to the received information, compute the sums of frequency, voltage, real and reactive power from (10a), (10b) and (12).
- 5: Update matrices $H_i, F_i, A_i, A_{eq,i}, B_i, B_{eq,i}$ from (13) according to the results of step 4 and the measurements/estimations $\{\omega_i(t_n), \omega_i^*(t_n), V_i(t_n), V_i^*(t_n), \delta\theta_i(t_n), P_i(t_n), Q_i(t_n)\}$.
- 6: Solve QP problem using QPKWIK algorithm.
- 7: **if** \mathbb{X}_i is feasible and $t < t_n + T_{sec}$ **then**
- 8: Extract $\Delta\omega_{s,i}(t_n), \Delta V_{s,i}(t_n)$ from \mathbb{X}_i .
- 9: **else**
- 10: $\Delta\omega_{s,i}(t_n) = 0, \Delta V_{s,i}(t_n) = 0$.
- 11: **end if**
- 12: Update controller outputs and send \mathbb{X}_i to neighbor DGs if it is feasible
- 13: **end for**

D. Quadratic Programming Formulation

From the cost function (12), and using (9a) and (10a) as constraints, it is possible to define the matrices/vectors $H_i, F_i, A_i, B_i, A_{eq,i}, B_{eq,i}$ to build a quadratic programming (QP) problem for each DG in the microgrid, as defined in (14). Then, the output vector \mathbb{X}_i is defined by (14), where the set of predicted variables is represented by $\mathbb{X}_{p,i}$ and the optimal control sequences $\mathbb{X}_{\Delta,i}$ are defined by (15) and (16).

$$\begin{aligned} \underset{\mathbb{X}_i}{\text{minimize}} \quad & J_i(t_n) := \frac{1}{2} \mathbb{X}_i^T H_i \mathbb{X}_i + F_i^T \mathbb{X}_i \\ \text{subject to} \quad & A_i \mathbb{X}_i \leq B_i \end{aligned} \quad (13)$$

$$\begin{aligned} & A_{eq,i} \mathbb{X}_i = B_{eq,i} \\ \mathbb{X}_i = \{ & \mathbb{X}_{p,i}, \mathbb{X}_{\Delta,i} \} \end{aligned} \quad (14)$$

$$\mathbb{X}_{p,i} = \{ \bar{\omega}_i(t_{n+k}), \bar{V}_i(t_{n+k}), \omega_i(t_{n+k}), V_i(t_{n+k}), \delta\theta_i(t_{n+k}), P_i(t_{n+k}), Q_i(t_{n+k}) \}_{k=1}^{N_y} \quad (15)$$

$$\mathbb{X}_{\Delta,i} = \{ \Delta\omega_{s,i}(t_{n+k-1}), \Delta V_{s,i}(t_{n+k-1}) \}_{k=1}^{N_u} \quad (16)$$

As mentioned in [14], a stable predictive control requires a feasible solution to the optimization problem. Note that (10c) to (10f) are related to the QP feasibility, ensuring that the system operates within physical limits over the whole prediction horizon. To ensure a feasible initial condition, the DMPC is enabled when the microgrid is operating around ω_0 and V_0 ; however, if a non-feasible solution is obtained to the QP problem, $\Delta\omega_{s,i}(t_{n+1})$ and $\Delta V_{s,i}(t_{n+1})$ are set to zero. In a black start scenario, this state is achieved when the primary control level operates without load.

The computational cost is also related to the QP feasibility. The range and final value constraints limit the feasible solution space of the QP problem; then, the computational cost to solve the problem is also reduced [14]. In this case, we use an efficient and stable variation of the classic active-set method called the QPKWIK algorithm to solve the QP problem (14) [23]. A description about how the QP problem is solved is included in Algorithm 1.

Although a stability analysis is beyond the scope of this paper, we suggest to the reader the comprehensive approach about DMPC stability presented on [24].

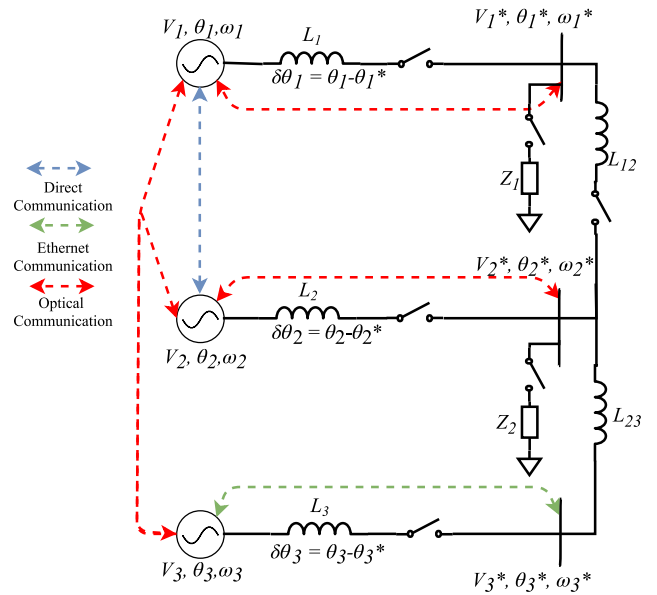


Fig. 2. Experimental microgrid diagram.

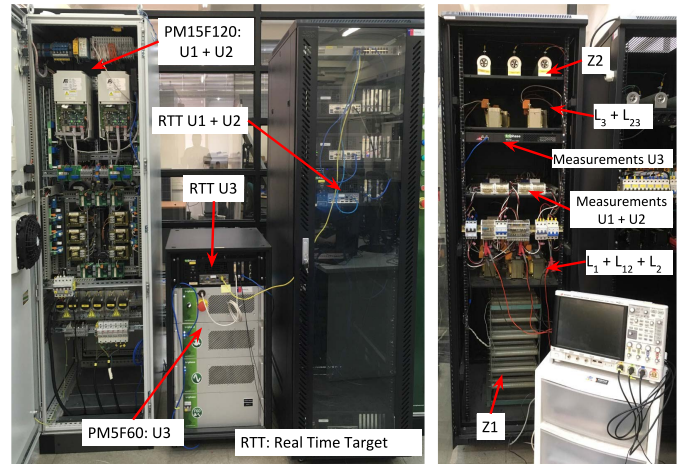


Fig. 3. Experimental setup.

IV. EXPERIMENTAL SETUP AND RESULTS**A. Experimental Setup**

To validate the proposed DMPC strategy, an experimental setup was built in the Microgrids Control Lab of the University of Chile. The setup uses PM15F120 and PM5F60 *Triphase* modules to emulate a three-DG microgrid. Each module is controlled by a real-time target (RTT) computer, where the DMPC for each DG is downloaded. External measurement devices were connected to the measurement nodes, and these devices directly communicate with their respective RTTs. A diagram of the setup is shown in Fig. 2, and a photo register is shown in Fig. 3. In Table I and Table II, electrical and droop parameters are presented.

The weighting factors used by the cost function were heuristically tuned, managing the tradeoff among the control objectives, and if required giving priority to one of the control objectives over the other objectives. The estimated delay corresponds to one sampling period on the secondary level and it

TABLE I
MICROGRID ELECTRICAL PARAMETERS

Parameter	Description	Value
T_{prim}	Primary Level Sampling Period	1/16E3 s
Z_1	Load 1	11 Ω
Z_2	Load 2	22 Ω
L_i	Coupling Inductance	2.5 mH
L_{ij}	Transmission Line Inductance	2.5 mH
ω_0	Nominal Frequency	314.159 rad/s
V_0	Nominal Voltage (peak)	150 V
ω_c	Cutoff Frequency - Droop Controller	2π rad/s

TABLE II
POWER CAPACITIES AND DROOP SLOPES

Power Capacities and Droop Slopes		DG ₁	DG ₂	DG ₃
S_{max} [KVA]	Power Capacity	2.4	1.92	1.2
$M_{p\omega}$ [$\frac{\text{rad}}{\text{s}\cdot\text{W}}$]	P- ω Droop Slope	-1E-4	-1.5E-4	-2.5E-4
M_{qv} [$\frac{\text{V}}{\text{VAR}}$]	Q-V Droop Slope	-1E-3	-1.5E-3	-1.8E-3

TABLE III
DMPC GENERAL PARAMETERS

Parameter	Description	Value
T_{sec}	Secondary Level Sampling Period	0.05 s
$\hat{\tau}_{ij}$	Estimated Communication Delay	0.05 s
N_y	Prediction Horizon	10
N_u	Control Horizon	10
V_{max}	Maximum Voltage	155V
V_{min}	Minimum Voltage	145V

TABLE IV
DMPC WEIGHTING FACTORS

Weighting Factors		DG ₁	DG ₂	DG ₃
λ_1 [$\frac{\text{s}}{\text{rad}}$] ²	Average Frequency Error	3E4	5E4	9E4
λ_2 [$\frac{1}{\text{V}}$] ²	Average Voltage Error	5E0	6E0	7E0
λ_3 [$\frac{\text{s}}{\text{rad}}$] ²	Frequency Control Action	8E4	8E4	9E5
λ_4 [$\frac{1}{\text{V}}$] ²	Voltage Control Action	5E3	5E3	5E3
λ_5 [$\frac{\text{VA}}{\text{W}}$] ²	Real Power Consensus	1.5E2	1.3E2	2E2
λ_6 [$\frac{\text{VA}}{\text{VAR}}$] ²	Reactive Power Consensus	5E3	2E3	1E3

is determined according to the delay requirement for control information shown in [25]. The DMPC general parameters and weighting factors are shown in Table III and Table IV. The PI inner loops gains and other parameters that are not relevant to DMPC are omitted in this paper.

Four scenarios were implemented with the experimental setup using the proposed DMPC. The first (base case) scenario shows the DMPC performance when the microgrid is disturbed with load changes. In the second scenario, a communication failure between DG₁ and DG₂ is forced while the microgrid is disturbed. The third scenario is a PnP test, where DG₃ is disconnected and reconnected to the microgrid. Finally, the fourth scenario shows the microgrid performance when the latency changes over the communication network.

B. Test Scenario 1 (Base Case)-Load Changes

This scenario tests the microgrid behavior using the proposed DMPC when several load changes are applied. In this case, the microgrid begins without load, and at $t = 38s$, load Z_1 is connected to the microgrid. At $t = 58s$, the total load in the microgrid is composed of Z_1 and Z_2 . Finally at

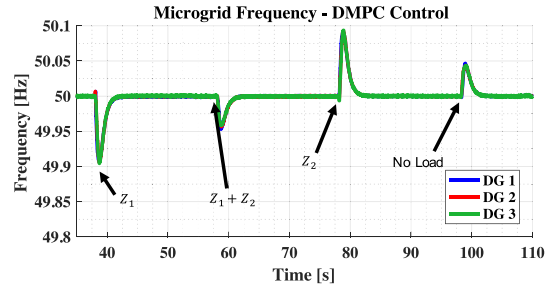


Fig. 4. Frequency regulation against load changes - DMPC base case.

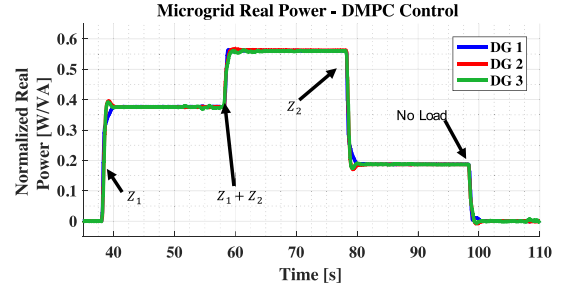


Fig. 5. Real power consensus against load changes - DMPC base case.

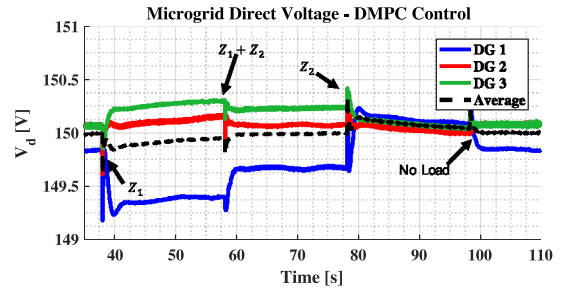


Fig. 6. Voltage regulation against load changes - DMPC base case.

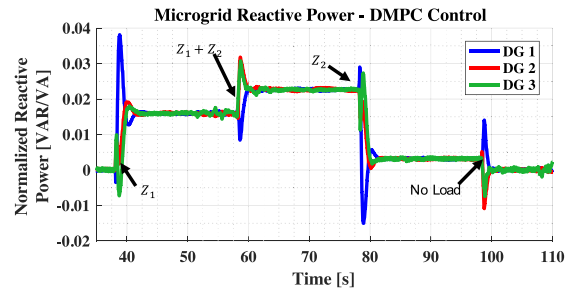


Fig. 7. Reactive power consensus against load changes - DMPC base case.

$t = 78s$ and $t = 98s$, the load is reduced to Z_1 and zero, respectively.

In Fig. 4 and Fig. 6, it is shown that the average frequency and average voltage are regulated; however, voltage deviations over each DG caused by the microgrid heterogeneity are observed. Fig. 5 and Fig. 7 show that the consensus of real and reactive power is achieved. In these figures, the power contribution of each DG is normalized with respect to its capacity.

Over the whole test, the microgrid is preserved as in Fig. 2, and the disturbances are limited to load changes. In this case,

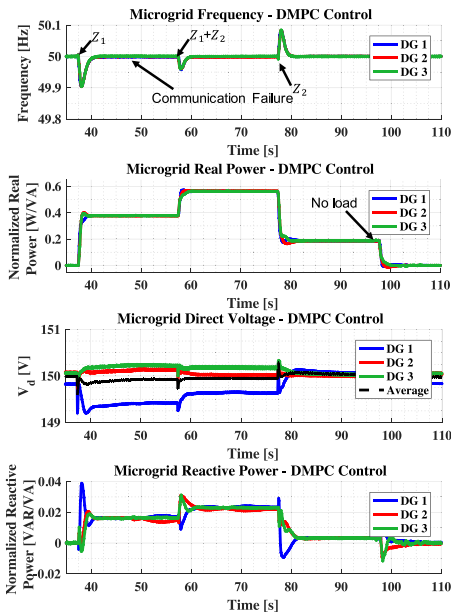


Fig. 8. Microgrid response against communication failure between DG₁ and DG₂.

the adjacency matrix is constant and given by (17).

$$A(t) = \begin{bmatrix} a_{11} & a_{12} & a_{13} \\ a_{21} & a_{22} & a_{23} \\ a_{31} & a_{32} & a_{33} \end{bmatrix} = \begin{bmatrix} 0 & 1 & 1 \\ 1 & 0 & 1 \\ 1 & 1 & 0 \end{bmatrix} \quad (17)$$

This test scenario shows the basic microgrid operation, and it is considered as a base case for comparisons with the following scenarios tested in this paper.

C. Test Scenario 2 - Communication Path Failure

This scenario adds to the base case a failure over the communication path between DG₁ and DG₂ at $t = 50s$. This failure is kept until the end of the test. This type of failure can be understood as a physical failure over the communication path or a simple data packet loss. In this case, as the adjacency matrix is a function of the information received for each controller, it is updated when the communication fails, preserving the average values.

The microgrid response is shown in Fig. 8. From the results, it is possible to state that the microgrid remains stable, achieving the four control objectives (frequency/voltage regulation and real/reactive power consensus) even when the communication path fails. This can be understood as a communication fault-tolerance feature of the proposed DMPC; however, as shown in Fig. 9, a difference in the transient state is observed when load changes are applied. This change is caused by the relationship between the adjacency matrix and the cost function (12); as the adjacency terms are updated, but not the weighting factors, the tuned parameters do not compensate for the load changes in the same manner as when the communication network is complete.

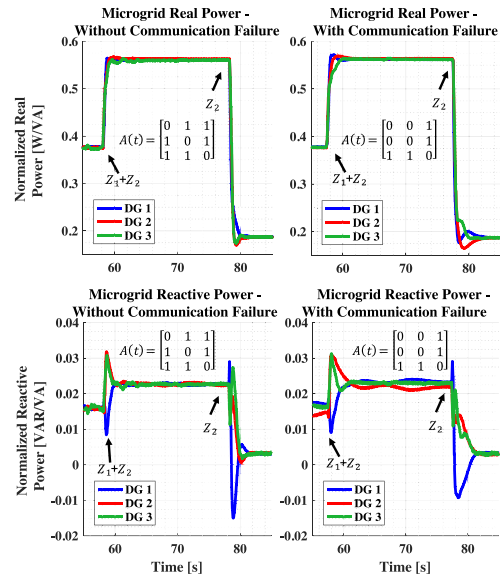


Fig. 9. Consensus detail - microgrid response against communication failure between DG₁ and DG₂.

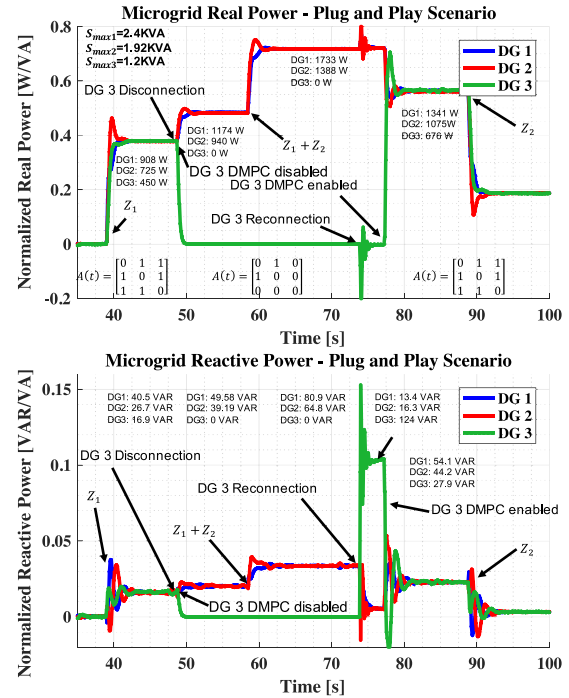


Fig. 10. Real Power (top) and Reactive Power (bottom) Behavior - Plug and Play Test.

D. Test Scenario 3 - Plug-and-Play Capability

This test shows the microgrid response when DG₃ fails and is disconnected (at $t \approx 49s$); after a synchronization sequence, it is reconnected to the microgrid (at $t \approx 75s$). When DG₃ is disconnected from the microgrid, its secondary control is disabled, and after the reconnection, it is re-enabled. Fig. 10 shows a power distribution according to the DGs connected to the microgrid. Because the adjacency matrix $A(t)$ depends on the information received by each DG, it is updated when DG₃ is disconnected and reconnected, therein adjusting the consensus and the average values in the optimization problem.

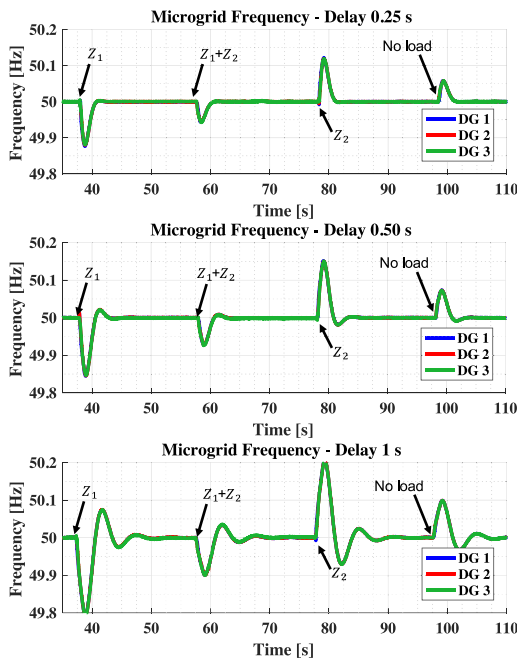


Fig. 11. Microgrid behavior with communication delays- frequency response- top: $\tau_{ij} = 0.25s$ middle: $\tau_{ij} = 0.5s$ bottom: $\tau_{ij} = 1s$.

Between $t \approx 75s$ and $t \approx 78s$, the real and reactive power contributions of DG₃ are not in consensus even though the DG₃ is connected to the microgrid. In this period, DG₃ is synchronized ($\delta\theta_3 = 0$), and its secondary controller is disabled; thus, according to (4) and (5), only the reactive power flow through L_3 is feasible. When the secondary controller is enabled on DG₃, the power consensus among the three units is re-established.

E. Test Scenario 4 - Communication Delay Response

This scenario compares the microgrid response at different values of τ_{ij} but preserving $\hat{\tau}_{ij}$ as one sampling period (0.05s). Although it is reported that emergent communication technologies used in microgrids have a latency of less than 100 ms [26], the microgrid performance was evaluated using a 1s delay as a worst-case scenario, because issues such as the weather or maintenance frequency affect the communication performance in rural/remote areas [27]. For each test, the same load changes from scenario 1 are applied. The results for frequency regulation and real power consensus are shown in Fig. 11 and Fig. 12, respectively.

From the results, it is possible to state that the microgrid response increases its overshoot and its settling time when the communication delay also increases; however, the microgrid achieves the control objectives even when the delay is 20-times the sampling period (T_{sec}).

The DMPC latency compensation is related to the rolling prediction/control horizons, the sampling period and the delay estimation $\hat{\tau}_{ij}$; however, either longer horizons or a shorter sampling period increase the computational effort. Even when the optimization problem is solved based on delayed information from neighboring DGs, the rolling horizon scheme

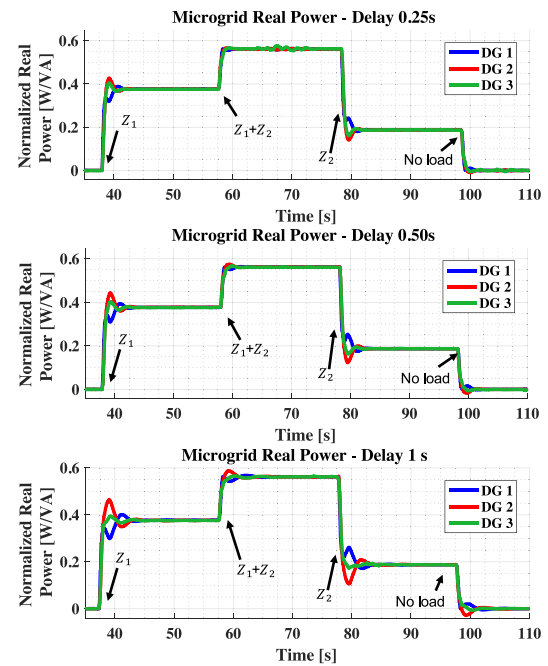


Fig. 12. Microgrid behavior with communication delays- real power response- top: $\tau_{ij} = 0.25s$ middle: $\tau_{ij} = 0.5s$ bottom: $\tau_{ij} = 1s$.

updates the control sequence each sampling period, compensating for latency effects even beyond the prediction horizon.

V. SCALABILITY AND COMPARISON WITH A DAPI CONTROLLER

To discuss the scalability of the proposed DMPC, a simulated microgrid with six DGs is built. The microgrid electrical model is developed with *Plecs blockset*, whereas the primary and secondary controllers, are implemented in a *MATLAB – Simulink* environment. This simulator is the closest to a real microgrid; thus details such as the inner loops, droop controllers, LC filters, resistive loads, and switch snubbers are also modeled.

For simulation purposes, the same electrical and general DMPC parameters as in the experimental case were considered, as shown in Table I and Table III, respectively. New generators DG₄, DG₅ and DG₆ were included with the same power capacities and droop slopes than DG₃, DG₂ and DG₁ respectively (Table II), and the DMPC weighting factors for the new DGs are shown in Table V. A diagram with the microgrid is shown in Fig. 13. Note that additional loads $Z_5 = Z_6 = (0.045 - 0.0637j)\Omega$ were included to increase the reactive power demand.

A. Scalability

DG₄, DG₅ and DG₆ were connected to the microgrid at $t = 20$, $t = 40$ and $t = 50$, considering DG₁, DG₂, DG₃, Z_1 and Z_2 previously connected and enabled, as shown in Fig. 14 and Fig. 15. Note that according to the average and consensus terms on (12) and (10a), the S_{jmax} values, as well as the number of units on the microgrid p , should be known for

TABLE V
DMPC WEIGHTING FACTORS

Weighting Factors		DG ₄	DG ₅	DG ₆
λ_1 $[\frac{s}{rad}]^2$	Average Frequency Error	9E4	5E4	3E4
λ_2 $[\frac{1}{V}]^2$	Average Voltage Error	7E0	6E0	5E0
λ_3 $[\frac{s}{rad}]^2$	Frequency Control Action	9E4	9E4	9E4
λ_4 $[\frac{1}{V}]^2$	Voltage Control Action	5E3	5E3	5E2
λ_5 $[\frac{VA}{W}]^2$	Real Power Consensus	4.0E2	6.5E2	2.5E2
λ_6 $[\frac{VA}{VAR}]^2$	Reactive Power Consensus	5E3	7E3	7E3

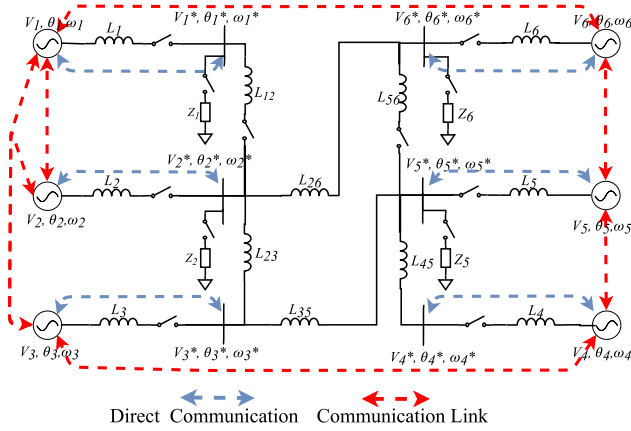


Fig. 13. Simulated microgrid diagram.

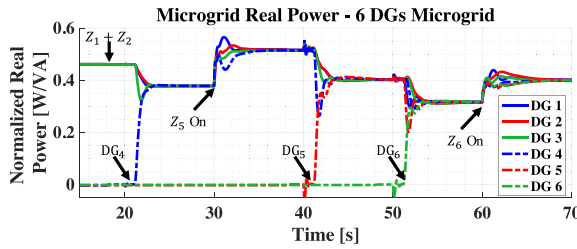


Fig. 14. Real Power behavior - simulated microgrid diagram.

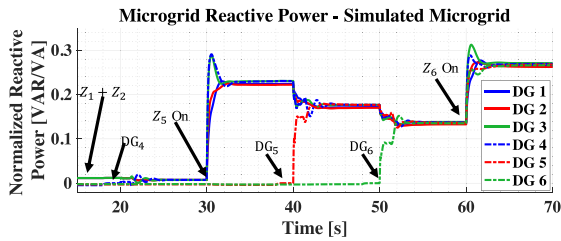


Fig. 15. Reactive power behavior - simulated microgrid diagram.

each DG. Updating this information is required only when a new DG is introduced to the microgrid. Then a broadcast message during the new DG commissioning stage, including the DG sub-index and its maximum apparent power is sufficient for the recognition of the new DG. This does not compromise the PnP capability of our proposal, because the DG can be disconnected or re-connected (after the initial connection) without a re-transmission of this message.

TABLE VI
DAPI PARAMETERS

DAPI Parameters		DG ₁	DG ₂	DG ₃	DG ₄	DG ₅	DG ₆
$K_{i,\omega}$ [s]	Integral Frequency Gain	1.08E-1	1.04E-1	8E-1	8E-1	1.04E-1	1.08E-1
$K_{i,v}$ [s]	Integral Voltage Gain	1E0	1E0	1E0	1E0	1E0	1E0
β_i [V]	Weighting Factor- Voltage Regulation	5E-1	1E-1	9.5E-1	4E-1	1E-1	1E-1
b_i [V]	Weighting Factor- Reactive Power Consensus	9E0	1.05E1	7.5E0	1.2E1	1.35E1	1.35E1

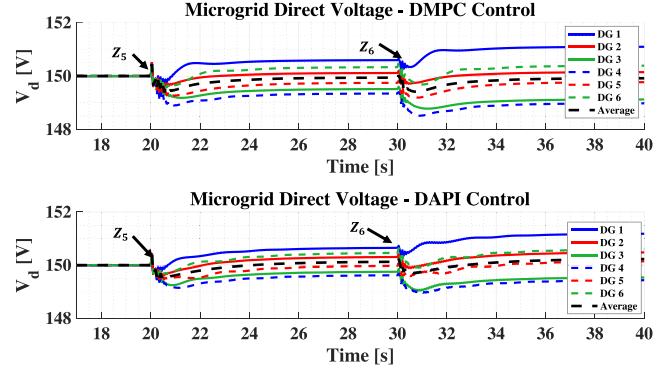


Fig. 16. Voltage response using DMPC (Top) and DAPI (Bottom) controllers.

B. Comparison With DAPI Controller

The DAPI is a distributed scheme based on PI controllers and has been widely reported for frequency and voltage regulation in microgrids. The main advantage of the DAPI is the inclusion of the consensus into the control law. A comparison between the proposed DMPC and the DAPI is justified because both schemes include regulation and consensus objectives, as well as, the communication network topology from the adjacency matrix. For an adequate comparison, the consensus variable for the DAPI controller for frequency regulation is switched to the real power, and the adjacency term is continuously updated. The discretized control law used for the DAPI scheme is shown in (18a). As explained in [6], $K_{i,\omega}$ and $K_{i,v}$ are the integral gains, whereas β_i , and b_i weight the trade-off between voltage regulation and reactive power consensus. (See the values on Table VI)

$$K_{i,\omega}\omega_{s,i}(t_n) = K_{i,\omega}\omega_{s,i}(t_{n-1}) - T_{sec}(\omega_i(t_n) - \omega_0) - T_{sec} \sum_{j=1, j \neq i}^p a_{ij}(t_n) \left(\frac{P_i(t_{n+k})}{|S_{i,max}|} - \frac{P_j(t_{n+k-\hat{\tau}_{ij}})}{|S_{j,max}|} \right) \quad (18a)$$

$$K_{i,v}V_{s,i}(t_n) = K_{i,v}V_{s,i}(t_{n-1}) - T_{sec}\beta_i(V_i(t_n) - V_0) - T_{sec} \sum_{j=1, j \neq i}^p b_i a_{ij}(t_n) \left(\frac{Q_i(t_{n+k})}{|S_{i,max}|} - \frac{Q_j(t_{n+k-\hat{\tau}_{ij}})}{|S_{j,max}|} \right) \quad (18b)$$

Fig. 16 and Fig. 17 show the voltage and reactive power responses, respectively, when Z_5 and Z_6 are connected to the microgrid. Note that, although the local voltage for each DG is similar for both schemes, the reactive power consensus is achieved when the DMPC is used. However, it is possible to achieve the reactive power consensus using DAPI scheme as well; but it implies a poor response for voltage regulation [6].

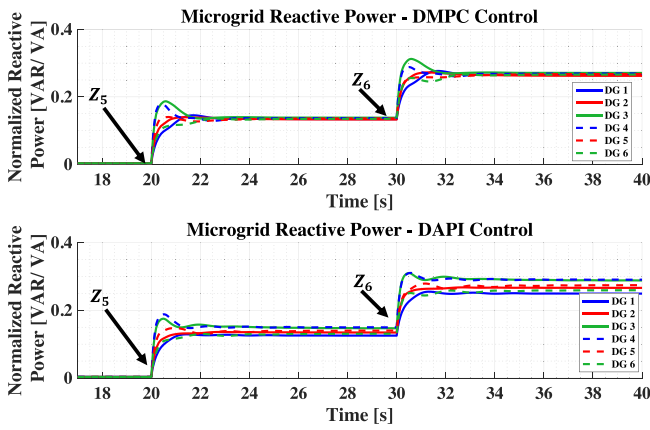


Fig. 17. Reactive power response using DMPC (Top) and DAPI (Bottom) controllers.

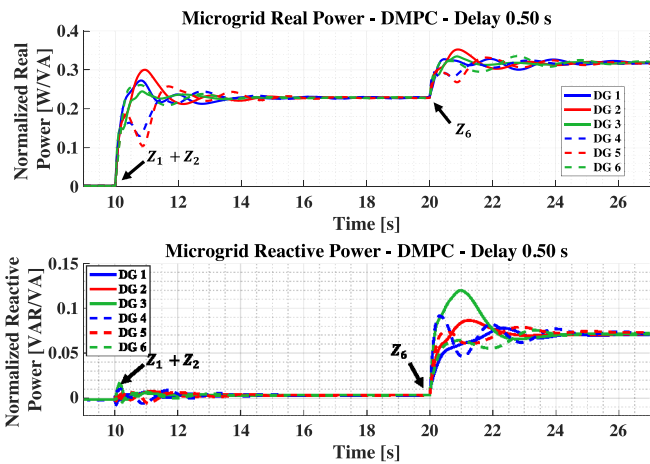


Fig. 18. Power behavior using DMPC with communication delay $\tau_{ij} = 0.5s$.

A second difference between the proposed DMPC and DAPI schemes is the latency tolerance. As was shown in Section IV-E, the rolling horizon feature and the latency estimation included in the optimization problem, allows the communication delay effect to be compensated. Moreover, the DAPI controller, does not possess a delay compensation mechanism; thus, the latency effect is evidenced as a more oscillatory response than the DMPC at the same value of τ_{ij} . In Fig. 18 and Fig. 19, the real and reactive power responses are shown for when Z_1 , Z_2 and Z_5 are connected to the microgrid and when a delay $\tau_{ij} = 0.5s$ is applied to the communication network. Note that although for both controllers the transient state is affected when the load changes, the proposed DMPC achieves the real and reactive power consensus; however, DAPI controller loses this feature, presenting oscillations for DG_1 and DG_6 .

VI. CONCLUSION AND FINAL REMARKS

In this paper, a distributed predictive controller for regulating the frequency and average voltage and achieving real and reactive power consensus in the microgrid was presented. The main contribution of this paper is the proposed model based on droop, power transfer and phase angle equations used to

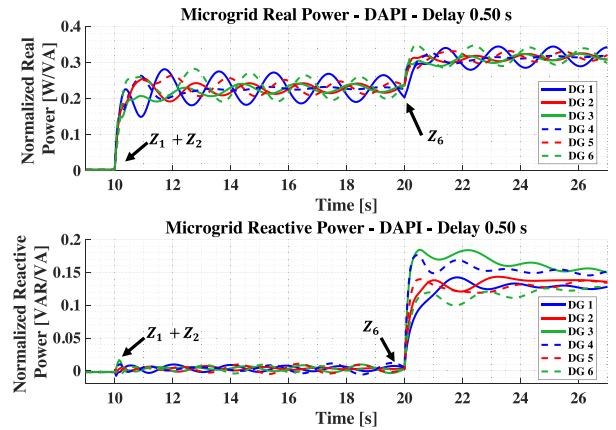


Fig. 19. Power behavior using DAPI with communication delay $\tau_{ij} = 0.5s$.

solve the DMPC. The proposed formulation includes explicit operational constraints to ensure the operation of the microgrid within feasible ranges, additionally, the model is able to modify its adjacency matrix in response to either electrical or communications disturbances.

The performed simulations and experimental tests show that the use of the proposed predictive controller allows achieving the regulation and consensus objectives satisfying the operational constraints. The proposed controller improves the microgrid performance against electrical disturbances, such as load changes or disconnecting/reconnecting of DGs (PnP capability), and communication issues such as latency and data packet losses.

Finally, as future work, the application of this type of DMPC to hybrid AC/DC microgrids with energy storage systems is suggested.

REFERENCES

- [1] R. J. Patton, C. Kambhampati, A. Casavola, P. Zhang, S. Ding, and D. Sauter, "A generic strategy for fault-tolerance in control systems distributed over a network," *Eur. J. Control*, vol. 13, nos. 2–3, pp. 280–296, Jan. 2007.
- [2] M. Tucci and G. Ferrari-Trecate, "A scalable line-independent design algorithm for voltage and frequency control in AC islanded microgrids," *CoRR*, vol. abs/1703.02336, pp. 1–17, Mar. 2017.
- [3] S. Rivero, F. Sarzo, and G. Ferrari-Trecate, "Plug-and-play voltage and frequency control of islanded microgrids with meshed topology," *IEEE Trans. Smart Grid*, vol. 6, no. 3, pp. 1176–1184, May 2015.
- [4] F. Bullo, *Lectures on Network Systems*, J. Cortes, F. Dorfler, and S. Martinez, Eds., Kindle Direct, 2018. [Online]. Available: <http://motion.me.ucsb.edu/book-Ins>
- [5] R. Olfati-Saber, J. A. Fax, and R. M. Murray, "Consensus and cooperation in networked multi-agent systems," *Proc. IEEE*, vol. 95, no. 1, pp. 215–233, Jan. 2007.
- [6] J. W. Simpson-Porco, Q. Shafiee, F. Dorfler, J. C. Vasquez, J. M. Guerrero, and F. Bullo, "Secondary frequency and voltage control of islanded microgrids via distributed averaging," *IEEE Trans. Ind. Electron.*, vol. 62, no. 11, pp. 7025–7038, Nov. 2015.
- [7] Y.-B. Zhao, X.-M. Sun, J. Zhang, and P. Shi, "Networked control systems: The communication basics and control methodologies," *Math. Problems Eng.*, vol. 2015, pp. 1–9, Feb. 2015.
- [8] C. Ahumada, R. Cardenas, D. Saez, and J. M. Guerrero, "Secondary control strategies for frequency restoration in islanded microgrids with consideration of communication delays," *IEEE Trans. Smart Grid*, vol. 7, no. 3, pp. 1430–1441, May 2016.
- [9] S. Liu, X. Wang, and P. X. Liu, "Impact of communication delays on secondary frequency control in an islanded microgrid," *IEEE Trans. Ind. Electron.*, vol. 62, no. 4, pp. 2021–2031, Apr. 2015.

- [10] Y. Xu, H. Sun, W. Gu, Y. Xu, and Z. Li, "Optimal distributed control for secondary frequency and voltage regulation in an islanded microgrid," *IEEE Trans. Ind. Informat.*, vol. 15, no. 1, pp. 225–235, Jan. 2019.
- [11] G. Chen and Z. Guo, "Distributed secondary and optimal active power sharing control for islanded microgrids with communication delays," *IEEE Trans. Smart Grid*, vol. 10, no. 2, pp. 2002–2014, Mar. 2019.
- [12] Y. Han, K. Zhang, H. Li, E. A. A. Coelho, and J. M. Guerrero, "MAS-based distributed coordinated control and optimization in microgrid and microgrid clusters: A comprehensive overview," *IEEE Trans. Power Electron.*, vol. 33, no. 8, pp. 6488–6508, Aug. 2018.
- [13] M. H. Andishgar, E. Gholipour, and R.-A. Hooshmand, "An overview of control approaches of inverter-based microgrids in islanding mode of operation," *Renew. Sustain. Energy Rev.*, vol. 80, pp. 1043–1060, Dec. 2017.
- [14] E. F. Camacho and C. Bordons, "Constrained model predictive control," in *Model Predictive Control* (Advanced Textbooks in Control and Signal Processing), 2nd ed. London, U.K.: Springer, 2007.
- [15] P. D. Christofides, R. Scattolini, D. M. de la Peña, and J. Liu, "Distributed model predictive control: A tutorial review and future research directions," *Comput. Chem. Eng.*, vol. 51, pp. 21–41, Apr. 2013.
- [16] R. M. Hermans *et al.*, "Assessment of non-centralised model predictive control techniques for electrical power networks," *Int. J. Control*, vol. 85, no. 8, pp. 1162–1177, Aug. 2012.
- [17] G. Zhuoyu, L. Shaoyuan, and Z. Yi, "Distributed model predictive control for secondary voltage of the inverter-based microgrid," in *Proc. 36th Chin. Control Conf. (CCC)*, Jul. 2017, pp. 4630–4634.
- [18] G. Lou, W. Gu, W. Sheng, X. Song, and F. Gao, "Distributed model predictive secondary voltage control of islanded microgrids with feedback linearization," *IEEE Access*, vol. 6, pp. 50169–50178, 2018.
- [19] K. Liu, T. Liu, Z. Tang, and D. J. Hill, "Distributed MPC-based frequency control in networked microgrids with voltage constraints," *IEEE Trans. Smart Grid*, to be published.
- [20] Z. Guo, H. Jiang, Y. Zheng, and S. Li, "Distributed model predictive control for efficient operation of islanded microgrid," in *Proc. Chin. Autom. Congr. (CAC)*, Oct. 2017, pp. 6253–6258.
- [21] Y. Han, H. Li, P. Shen, E. A. A. Coelho, and J. M. Guerrero, "Review of active and reactive power sharing strategies in hierarchical controlled microgrids," *IEEE Trans. Power Electron.*, vol. 32, no. 3, pp. 2427–2451, Mar. 2017.
- [22] P. Kundur, *Power System Stability and Control*. New York, NY, USA: McGraw-Hill Educ., 1994.
- [23] C. Schmid and L. T. Biegler, "Quadratic programming methods for reduced Hessian SQP," *Comput. Chem. Eng.*, vol. 18, no. 9, pp. 817–832, Sep. 1994.
- [24] C. Conte, M. N. Zeilinger, M. Morari, and C. N. Jones, "Cooperative distributed tracking MPC for constrained linear systems: Theory and synthesis," in *Proc. 52nd IEEE Conf. Decis. Control*, Dec. 2013, pp. 3812–3817.
- [25] S. Marzal, R. Salas, R. González-Medina, G. Garcerá, and E. Figueres, "Current challenges and future trends in the field of communication architectures for microgrids," *Renew. Sustain. Energy Rev.*, vol. 82, pp. 3610–3622, Feb. 2018.
- [26] C. Kalalas, L. Thrybom, and J. Alonso-Zarate, "Cellular communications for smart grid neighborhood area networks: A survey," *IEEE Access*, vol. 4, pp. 1469–1493, 2016.
- [27] W. Wang, Y. Xu, and M. Khanna, "A survey on the communication architectures in smart grid," *Comput. Netw.*, vol. 55, no. 15, pp. 3604–3629, Oct. 2011.



Juan S. Gómez was born in Bogotá, Colombia. He received the B.Sc. degree in electronic engineering from the Universidad Distrital Francisco José de Caldas, Bogotá, in 2011. He is currently pursuing the Ph.D. degree with the Microgrids Control Lab, Department of Electrical Engineering, University of Chile. He was Project Engineer with Colombian Oil and Gas Industry, where he is a Specialist Automation Engineer from 2010 to 2016. His research interests are focused mainly on microgrids control, networked control systems, renewable energies, and model-based predictive control.



Doris Sáez (S'93–M'96–SM'05) was born in Panguipulli, Chile. She received the M.Sc. and Ph.D. degrees in electrical engineering from the Pontificia Universidad Católica de Chile, Santiago, Chile, in 1995 and 2000, respectively.

She is currently a Full Professor with the Department of Electrical Engineering, University of Chile, Santiago. She has coauthored the books entitled *Hybrid Predictive Control for Dynamic Transport Problems* (Springer-Verlag, 2013) and the *Optimization of Industrial Processes at Supervisory Level: Application to Control of Thermal Power Plants* (Springer-Verlag, 2002). Her research interests include predictive control, fuzzy control design, fuzzy identification, control of power generation plants, and control of transport systems. She is an Associate Editor of the IEEE TRANSACTIONS ON FUZZY SYSTEMS and the *IEEE Control Systems Magazine*.



John W. Simpson-Porco (S'11–M'16) received the B.Sc. degree in engineering physics from Queens University, Kingston, ON, Canada, in 2010, and the Ph.D. degree in mechanical engineering from the University of California at Santa Barbara, Santa Barbara, CA, USA, in 2015.

He was a Visiting Scientist with the Automatic Control Laboratory, ETH Zürich, Zürich, Switzerland. He is currently an Assistant Professor of electrical and computer engineering with the University of Waterloo, Waterloo, ON, Canada. His research focuses on the control and optimization of multiagent systems and networks, with applications in modernized power grids.

Prof. Simpson-Porco was a recipient of the 2012–2014 IFAC Automatica Prize and the Center for Control, Dynamical Systems, and Computation Best Thesis Award and Outstanding Scholar Fellowship.



Roberto Cárdenas (S'95–M'97–SM'07) was born in Punta Arenas, Chile. He received the B.S. degree from the University of Magallanes, Punta Arenas, in 1988, and the M.Sc. and Ph.D. degrees from the University of Nottingham, Nottingham, U.K., in 1992 and 1996, respectively. He was a Lecturer with the University of Magallanes from 1989 to 1991 and from 1996 to 2008. From 1991 to 1996, he was with the Power Electronics Machines and Control Group, University of Nottingham. From 2009 to 2011, he was with the Electrical Engineering Department,

University of Santiago, Santiago, Chile. He is currently a Full Professor of power electronics and drives with the Electrical Engineering Department, University of Chile, Santiago. His current research interests include the control of electrical machines, variable speed drives, and renewable energy systems.